Multiple histogram reweighting method for the surface tension calculation

A. Ghoufi,[1] F. Goujon,[2] V. Lachet,[1] and P. Malfreyt[2,a)]
[1]*IFP, 1-4 Av. de Bois Préau, 92852 Rueil Malmaison Cedex, France*
[2]*Laboratoire de Thermodynamique des Solutions et des Polymères, UMR CNRS 6003, Université Blaise Pascal, 63177 Aubière Cedex, France*

(Received 30 November 2007; accepted 11 March 2008; published online 21 April 2008)

The multiple histogram reweighting method takes advantage of calculating ensemble averages over a range of thermodynamic conditions without performing a molecular simulation at each thermodynamic point. We show that this method can easily be extended to the calculation of the surface tension. We develop a new methodology called multiple histogram reweighting with slab decomposition based on the decomposition of the system into slabs along the direction normal to the interface. The surface tension is then calculated from local values of the chemical potential and of the configurational energy using Monte Carlo (MC) simulations. We show that this methodology gives surface tension values in excellent agreement with experiments and with standard *NVT* MC simulations in the case of the liquid-vapor interface of carbon dioxide. © *2008 American Institute of Physics*. [DOI: 10.1063/1.2904460]

I. INTRODUCTION

The calculation of the surface tension using molecular simulation can be performed using different methodologies. The most natural method consists in modeling two coexisting phases in physical contact in a liquid-slab arrangement. This methodology takes advantage of providing a molecular description of the interfacial region. However, it depends on the set up conditions (truncation procedures,[1–3] cutoff radius,[1,4] long range corrections (LRCs),[2,4] and size of the simulation cell[4,5]). Other methodologies avoid the need to establish an interface. These approaches are based on the thermodynamic definition of the surface tension and express the surface tension from the contribution to the free energy due to the formation of the interface.

Within the framework of free energy methods, the grand canonical transition matrix Monte Carlo[6,7] (GC-TMMC) method determines the density dependence of the free energy of a fluid at a given temperature. When the GC-TMMC method is associated with the Binder approach,[8] the surface tension is related to the free energy barrier between vapor and liquid phases, which is calculated from a GC-TMMC probability distribution.[9–12] Within the Binder approach, the density dependence of the system can be explored with the aid of a histogram reweighting method.[13,14] This approach has been successfully applied on Lennard-Jones[6,9,15] (LJ), square well,[10] *n*-alkanes,[11] and LJ mixtures[16] and is particularly attractive at relatively high temperatures along the liquid-vapor saturation line. A second general method based on the free energy of the system uses the ghost interface technique[17] in conjunction with a modified Gibbs ensemble method for the simulation of adjacent coexisting phases. All these methods do not require the physical presence of the interface.

The molecular simulations of the two-phase systems with the explicit presence of the interface allow us to calculate the surface tension and to describe the interfacial region at a molecular level. This leads to heterogeneous systems where a nonuniformity of the density number takes place along the direction normal to the interface. These two-phase simulations are challenging and special attention has to be paid on a certain number of factors: the time required to stabilize the formation of the interface, the validation of the thermodynamic equilibria (thermal, mechanical, and chemical), the truncation effects involved in the calculation of the potential and corresponding force, and the procedures used for calculating the electrostatic contributions. The influence of these factors[1–5,18] on the initial setup of the simulations has been extensively studied during these past years.

A certain number of operational expressions have been established for the surface tension calculation. The most general working expression uses macroscopic normal and tangential pressures, which can be related to the derivative of the pair potential. The final form has been obtained by Kirkwood and Buff[19–22] (KB) and gives a macroscopic scalar surface tension. In the case of a planar liquid-vapor interface lying in the x,y plane, the density gradient takes place in the z direction normal to the surface. The surface tension can be expressed as $\int_{-\infty}^{\infty}(p_N(z)-p_T(z))dz$, where $p_N(z)$ and $p_T(z)$ are local values of the normal and tangential components of the pressure tensor, respectively. Expressing the surface tension as a function of the local components of the pressure allows us to use a local $\gamma(z)$ defined as $\int_{-\infty}^{z}(p_N(z)-p_T(z))dz$. The use of $\gamma(z)$ is a key element to check the validity of the calculation concerning the stabilization of the interfaces, the independence between the two interfaces, and the constancy of $\gamma(z)$ in the bulk phases. We note that there are many ways of expressing the local components of the pressure, which depend on the contour joining two interacting molecules. Irving and Kirkwood[23–26] (IK) used a straight line to join the two particles. This choice is the most natural and the one generally made. Nevertheless, the scalar value of surface tension is invariant to the choice of the pressure tensor. Until recently,

a)Author to whom correspondence should be addressed. Electronic mail: patrice.malfreyt@univ-bpclermont.fr.

only the method of Irving and Kirkwood was designed to provide a profile of the surface tension. Both methods (KB and IK) are based on the mechanical definition on the surface tension.

Recently, the "test-area"[27] (TA) method based on the perturbation formalism was proposed for the calculation of the surface tension. This method takes advantage of expressing the surface tension as a difference in energy between a reference state and a perturbed state characterized by an infinitesimal increase or decrease in the surface. However, the aspect of the local surface tension was missing within the Kirkwood–Buff expression and the TA method. This led us to establish the local expression of the surface tension calculated from the test-area approach[3] and to propose the local version of the surface tension resulting from the virial route (KBZ) in a recent work where KB refers to the Kirkwood-Buff definition and Z indicates the direction of the gradient density.[28]

The surface tension can also be calculated from the amplitude of capillary waves[23,29] at the liquid-vapor interface. The interface Hamiltonian[30] can be linearized; it is found that the square of the interfacial thickness is related to the surface tension. It is then possible to calculate the surface tension from a series of simulations for systems of different interface sizes. This technique has been applied recently to the surface tensions of a polymer melt[30] and of water.[31]

Additionally, the use of truncated potential requires adding LRCs to the thermodynamic properties and an inconsistent treatment of the LRCs to the surface tension can lead to conflicting results between the different methods. It is also essential to associate an appropriate expression of the tail correction with that of the intrinsic part of the surface tension. A certain number of expressions for calculating the LRC contributions of the surface tensions were developed.[32–37] Some of them[34–37] express the LRC contributions of the surface tension along the direction perpendicular to the interface. Our conclusions from a previous work[3] showed that the different methods (IK, TA, and KB) matched very well as long as appropriate LRC contributions were included in the calculation. We have also proposed the operational expression of the LRC profile[3] of the surface tension within the TA approach. It is now well established that the LRCs of the surface tension can represent up to 30% of the total value for cutoff radii similar to those used for homogeneous systems.

The methodology consisting in calculating the surface tension from a direct Monte Carlo (MC) simulation with coexisting phases in physical contact is time consuming and a systematic study of the temperature dependence of these interfacial properties may represent a relatively cumbersome task. In order to improve the efficiency of the calculation, we aim at extending the histogram reweighting method, originally proposed to assess bulk properties, to the calculation of interfacial properties.

The multiple histogram reweighting (MHR) technique[13,14] represents a powerful technique to extend the information obtained from MC simulations to different thermodynamic states. Additionally, this method increases the accuracy in the evaluation of the nonreweighted thermodynamic properties.

Throughout this paper, we propose the development of the MHR methodology devoted to the surface tension using the IK definition. The methodology developed here can be used with other definitions of the surface tension as, for instance, the local definition of the TA method and the KBZ approach. We apply the developed methods to the calculation of the surface tension of the liquid-vapor interface of carbon dioxide.

The paper is organized as follows. Section II contains the description of the IK definition for the surface tension calculation and the standard histogram reweighting methods. Section III presents the MHR method we have developed for a two-phase system. Section IV discusses the results of the surface tension as a function of the technique used, and Sec. V contains our conclusions.

II. THEORETICAL BACKGROUND

A. Surface tension calculation

In the case of a system baring two planar liquid-vapor surfaces lying in the x,y plane, where the heterogeneity takes place in the z axis normal to the interfaces, the surface tension can be calculated from the integration of the difference of the normal and tangential components of the pressure tensor of IK (Refs. 19 and 23–26) across both interfaces according to

$$\gamma_{\mathrm{IK}} = \frac{1}{2}\int_{-L_z/2}^{+L_z/2} dz(p_N(z) - p_T(z)), \tag{1}$$

where $p_N(z)$ and $p_T(z)$ are the z components of the normal and tangential pressure tensors, respectively, calculated using Eq. (2). This operational expression also provides a profile of the surface tension $\gamma_{\mathrm{IK}}(z_k)$ defined as $(p_N(z_k)-p_T(z_k))\delta z$. The total surface tension is then calculated via the half sum of the local surface tensions $\gamma_{\mathrm{IK}}(z_k)$,

$$p_{\alpha\beta}(z_k) = \langle\rho(z_k)\rangle k_B T\mathbf{I} - \frac{1}{A}\left\langle \sum_{i=1}^{N-1}\sum_{j>i}^{N} (\mathbf{r}_{ij})_\alpha(\mathbf{r}_{ij})_\beta \frac{1}{r_{ij}}\frac{dU(r_{ij})}{dr_{ij}}\frac{1}{|z_{ij}|} \times \theta\left(\frac{z_k - z_i}{z_{ij}}\right)\theta\left(\frac{z_j - z_k}{z_{ij}}\right)\right\rangle, \tag{2}$$

where $\mathbf{I}$ is the unit tensor and T is the input temperature. α and β represent x, y, or z directions. $\theta(x)$ is the unit step function defined by $\theta(x)=0$ when $x<0$ and $\theta(x)=1$ when $x \geqslant 0$. A is the surface area normal to the z axis. The distance z_{ij} between two molecular centers of mass is divided into N_s slabs of thickness δz. Following IK, the molecules i and j give a local contribution to the pressure tensor in a given slab if the line joining i and j crosses, starts, or finishes in the slab. Each slab has $1/N_s$ of the total contribution from the i-j interaction. The normal component $p_N(z_k)$ is equal to $p_{zz}(z_k)$, whereas the tangential component is given by $\frac{1}{2}(p_{xx}(z_k) + p_{yy}(z_k))$. We adopt the molecular definition of the pressure

tensor using the center-of-mass definition. This operational expression also provides a profile of $(p_N(z_k)-p_T(z_k))\delta z$. The corresponding LRCs are calculated by Eq. (3) as proposed by Guo and Lu,[35]

$$\gamma_{\mathrm{IK,LRC}}(z_k)=\frac{\pi}{2}\rho(z_k)\delta_z\int_{r_c}^{\infty}dr\int_{-r}^{r}d\Delta\, z\sum_{i=1}^{N_s}[\rho(z_{k-i})-\rho(z_{k-i+1})]\frac{dU_{\mathrm{LJ},m}}{dr}[r^2-3(\Delta z)^2]. \tag{3}$$

Δz is the difference $(z-z_k)$ and varies between $-r$ and r. N_s is the number of slabs between z_k and z. The first term is similar to that used in a homogeneous system except for the use of a number of density $\rho(z_k)$ depending on z_k. The second term takes into account that each slab z_k is surrounded with slabs of different local densities. In this relation, $\rho(z_k)$ is the local density of the z_k slab and r represents the distance between the center of mass of two molecules. In Eq. (3), $U_{\mathrm{LJ},m}$ is defined as

$$U_{\mathrm{LJ},m}(r)=\sum_{a=1}^{N_a}\sum_{b=1}^{N_b}4\epsilon_{ab}\left[\left(\frac{\sigma_{ab}}{r}\right)^{12}-\left(\frac{\sigma_{ab}}{r}\right)^{6}\right], \tag{4}$$

where N_a and N_b represent the number of force centers in molecules a and b, respectively.

B. Single histogram reweighting

The histogram reweighting[13,38] method is a powerful technique that consists in extending the information extracted from a single MC simulation at an inverse temperature β to different temperatures. The canonical partition function Z_{NVT} can be expressed in terms of density of states as

$$Z_{NVT}=\sum_{\{\alpha\}}\exp(-E(\{\alpha\}))=\sum_{E}n(E)\exp(-\beta E), \tag{5}$$

where $\Sigma_{\{\alpha\}}$ represents the summation on the available states $(\{\alpha\})$ and $n(E)$ is the density of states of energy E. β is the inverse temperature defined as $1/k_BT$, where k_B is the Boltzmann constant. At T', the canonical partition function becomes

$$Z_{NVT'}=\sum_{E}n(E)\exp(-\beta' E) \tag{6a}$$

$$=\sum_{E}n(E)\exp(-\beta E)\exp(-(\beta'-\beta)E). \tag{6b}$$

The average of the observable X in the canonical ensemble at T' using the single histogram technique is given by

$$\langle X\rangle_{\beta'}=\frac{\Sigma_E X(E)n(E)\exp(-\beta' E)}{\Sigma_E n(E)\exp(-\beta' E)} \tag{7a}$$

$$=\frac{\Sigma_E X(E)n(E)\exp(-(\beta'-\beta)E)\exp(-\beta E)}{\Sigma_E n(E)\exp(-(\beta'-\beta)E)\exp(-\beta E)}. \tag{7b}$$

The counts of occurrence of energy $H(E)$ can be determined up to a constant $C(T)$ from the following expression:

$$H(E)=C(T)n(E)\exp(-\beta E), \tag{8}$$

where the constant $C(T)$ is only dependent on T. The average value of the X property using the single histogram method thus becomes

$$\langle X\rangle_{\beta'}=\frac{\Sigma_E X(E)H(E)\exp(-(\beta'-\beta)E)}{\Sigma_E H(E)\exp(-(\beta'-\beta)E)}. \tag{9}$$

Single histogram reweighting gives reliable results only over a limited range of energies. If β' differs too much from β, the peak of the reweighted histogram will be shifted to the tails of the measured histogram, where the statistical uncertainty is high. In this case, it is recommended to use the MHR methodology outlined by Ferrenberg and Swendsen.[14]

C. MHR

The MHR method takes advantage of collecting a series of histograms of the energy at nearby temperature overlap. We perform a series of R MC simulations in the canonical ensemble (NVT_i) corresponding to a different β_i inverse temperature. During these simulations we build a histogram $h_i(E)$ of the number of times that an energy E is observed, which is related to the density of states, $n(E)$. The true distribution of no weighted energy is expressed as

$$H_i(E)=\frac{n(E)\exp(-\beta_i E)}{\Sigma_E n(E)\exp(-\beta_i E)}. \tag{10}$$

The reduced free energy f_i is given by $f_i=-\ln\Sigma_E n(E)\exp(-\beta_i E)$, thus $\exp(-f_i)=\Sigma_E n(E)\exp(-\beta_i E)$. By using this expression, Eq. (10) can be rewritten as

$$H_i(E)=\frac{n(E)}{\exp(\beta_i E-f_i)}. \tag{11}$$

If we weight this distribution by the number of samples N_i in the simulation i, we obtain

$$\frac{h_i(E)}{N_i}=\frac{n(E)}{\exp(\beta_i E-f_i)}\Rightarrow n(E)=\frac{h_i(E)}{N_i}\exp(\beta_i E-f_i), \tag{12}$$

where $n(E)$ is calculated at a given inverse temperature β_i.

If we calculate $n(E)$ from different temperatures β_i, we combine R MC simulations and weight $n(E)$ by $p_i(E)$ as

$$n(E)=\sum_{i}^{R}\frac{p_i(E)h_i(E)}{N_i}\exp(\beta_i E-f_i)\quad\text{with}\sum_{i}^{R}p_i(E)=1, \tag{13}$$

where $p_i(E)$ indicates the relative weight of E by considering all simulations. $H_i(E)=p_i(E)h_i(E)$, where $p_i(E)$ is calculated by minimizing the error in $n(E)$ $(\delta^2 n(E))$ by using the Lagrange multipliers. We define $p_i(E)$ as follows:

$$p_i(E)=\frac{N_i\exp(-(\beta_i E-f_i))}{\Sigma_j^R N_j\exp(-(\beta_j E-f_j))}. \tag{14}$$

The improved estimate for the density of states becomes

$$n(E) = \frac{\Sigma_i^R h_i(E)}{\Sigma_j^R N_j \exp(-(\beta_j E - f_j))}. \quad (15)$$

The calculation of the free energy f_k at inverse temperature k is found self-consistently by iterating Eq. (16). Let us recall that k denotes one of the reference systems and varies from 1 to R, where R is the total number of independent MC simulations.

$$\exp(-f_k) = \sum_E n(E)\exp(-\beta_k E)$$

$$= \sum_E \frac{\Sigma_i^R h_i(E)}{\Sigma_j^R N_j \exp(-(\beta_j E - f_j))} \exp(-\beta_k E). \quad (16)$$

Once the value of f_k is obtained, we can calculate $n(E)$ and estimate the average of the observable X at the inverse temperature β according to

$$\langle X\rangle_\beta = \frac{\Sigma_E X(E) n(E)\exp(-\beta E)}{\Sigma_E n(E)\exp(-\beta E)}, \quad (17)$$

where $\langle X\rangle_\beta$ denotes the average of the X property at the β target inverse temperature.

We may express the expressions given in Eqs. (16) and (17) without building the histograms of energy and performing the sum over E first.[39] By using this methodology, the calculation of f_k can be done using Eqs. (18a) and (18b), and in a more operational expression, using Eq. (18c) as follows:

$$\exp(-f_k) = \sum_i^R \sum_E \frac{h_i(E)\exp(-\beta_k E)}{\Sigma_j^R N_j \exp(-(\beta_j E - f_j))} \quad (18a)$$

$$= \sum_i^R \sum_E \frac{h_i(E)}{\Sigma_j^R N_j \exp(-((\beta_j - \beta_k)E - f_j))} \quad (18b)$$

$$= \sum_i^R \sum_\alpha \frac{1}{\Sigma_j^R N_j \exp(-((\beta_j - \beta_k)E_{i\alpha} - f_j))}, \quad (18c)$$

where α in Eq. (18c) represents the α configuration in the i MC calculation. Whereas the average of the observable X requires in Eq. (19) the calculation of the histograms of E, the new operational expression of Eq. (20) uses the fact that the reweighted average of X can be performed without histograms as follows:

$$\langle X\rangle_\beta = \frac{\Sigma_E X(E)(\Sigma_i^R h_i(E))(\Sigma_j^R N_j \exp(-(\beta_j E - f_j)))^{-1}\exp(-\beta E)}{\Sigma_E (\Sigma_i^R h_i(E))(\Sigma_j^R N_j \exp(-(\beta_j E - f_j)))^{-1}\exp(-\beta E)}, \quad (19)$$

$$\langle X\rangle_\beta = \frac{\Sigma_i^R \Sigma_\alpha X_{i\alpha}(\Sigma_j^R N_j \exp(-((\beta_j - \beta)E_{i\alpha} - f_j)))^{-1}}{\Sigma_i^R \Sigma_\alpha (\Sigma_j^R N_j \exp(-((\beta_j - \beta)E_{i\alpha} - f_j)))^{-1}}. \quad (20)$$

III. HISTOGRAM REWEIGHTING METHODOLOGY FOR A TWO-PHASE SYSTEM

A. Multiple histogram reweighting for each slab (MHRS)

In the case of the simulation of a planar liquid-vapor surface lying in the x, y plane where a heterogeneity takes place in the z axis normal to the interface, we expect a dependence of the thermodynamic properties only in this z direction. This nonuniformity of the density imposes accounting for some local definitions of thermodynamic properties (pressure and energy density). We have also established in previous papers the uniformity of the local chemical potential, temperature, and pressure components for the liquid-vapor interfaces of *n*-alkanes. It is then very appropriate to develop a local version of the MHR method for the surface tension calculation. Additionally, when we focus on the fluctuations of the total energy of the simulation box during a MC simulation, we observe that they are very weak, and MC simulations of a two-phase system require very large systems to stabilize the interface. The two criteria, large fluctuations of the energy and a relatively small system, are important factors contributing to the efficiency of the MHR methodology. To evaluate the importance of fluctuations, we define the following coefficient: $r = \delta E/\langle E\rangle$. In the case of the liquid-vapor interface of carbon dioxide at 238 K, r is equal to 2.3×10^{-2} for the total simulation box, whereas it is equal to 0.6 and 3.8 for each slab of the liquid and vapor phases, respectively. As concerns the determination of the coexistence curves of tiophene using grand canonical MC combined with histogram reweighting methods,[40] r is equal to 0.7 and 2.4 in the liquid and vapor phases, respectively. We show that it is possible to converge to the same values of r when the system is decomposed into slabs. In what follows, we extend the MHR methodology to systems with slab decompositions (MHRS).

Let us recall that the MC simulation is carried out in the constant-*NVT* ensemble. The simulation box is divided into N_s slabs of width δz and volume $V_s = L_x L_y \delta z$. The total number of molecules N is constant, whereas the number of molecules N_{z_k} in each slab fluctuates within the simulation. This is equivalent to fixing the chemical potential μ_{z_k} of the considered species at each z_k position. The grand canonical partition function of the slab z_k can be written as

$$\Xi(\mu_{z_k}, V_{zk}, \beta) = \sum_{N_{z_k}} \sum_{U_{z_k}} \Omega(N_{z_k}, V_{zk}, \beta) \exp(-\beta(U_{z_k} - \mu_{z_k} N_{z_k})), \tag{21}$$

where μ_{z_k} is the chemical potential of the slab at z_k, β is the inverse temperature, U_{z_k} is the energy of the slab at z_k, and $\Omega(N_{z_k}, V_z k, \beta)$ is the canonical density of states. Writing Eq. (21) amounts to defining a local grand potential partition function. This leads to assuming the absence of correlations between neighboring slabs. In this case, all the slabs can be treated independently. The partition function of the system in the *NVT* ensemble can be expressed as

$$\prod_{z_k} \Xi(\mu_{z_k}, V_{zk}, T_{z_k}) \simeq \sum_{N} [\exp(\beta\mu N) Q(N, V, \beta)]. \tag{22}$$

Assuming the existence of this local partition function and satisfying the following criteria, $N = \Sigma_{i=1}^{N_s} N_{z_i}$ and $\int_V dz_k U_{z_k} = U$, it is then possible to establish the expression given in Eq. (22). The different steps leading to the final expression of Eq. (22) are given in Appendix A. The existence of the local partition function allows the application of the MHR methodology to each slab. If we follow the same procedure as that used for the MHR in the canonical ensemble, we obtain the expressions of Eqs. (23) and (24). An accurate demonstration has been performed by Pérez-Pellitero *et al.*[39] and Shi and Johnson[41] in the μVT ensemble.

$$\exp(-f_{l,z_k}) = \sum_{i}^{R} \sum_{\alpha} \left(\sum_{j}^{R} N_j \exp(-((\beta_j - \beta_l) E_{i\alpha,z_k} - n_{i\alpha,z_k}(\beta_j \mu_{j,z_k} - \beta_l \mu_{l,z_k}) - f_{j,z_k})) \right)^{-1}, \tag{23}$$

where l denotes the reference systems.

$$\langle X \rangle_{\beta,z_k} = \frac{\Sigma_i^R \Sigma_\alpha X_{i\alpha,z_k} (\Sigma_j^R N_j \exp(-((\beta_j - \beta) E_{i\alpha,z_k} - n_{i\alpha,z_k}(\beta_j \mu_{j,z_k} - \beta\mu_{\beta,z_k}) - f_{j,z_k})))^{-1}}{\Sigma_i^R \Sigma_\alpha (\Sigma_j^R N_j \exp(-((\beta_j - \beta) E_{i\alpha,z_k} - n_{i\alpha,z_k}(\beta_j \mu_{j,z_k} - \beta\mu_{\beta,z_k}) - f_{j,z_k})))^{-1}}, \tag{24}$$

where l varies from 1 to R, and μ_{β,z_k} is the total chemical potential of the slab k at the inverse target temperature β. $E_{i\alpha,z_k}$ is the energy of the slab at the position z_k at the inverse temperature β_i for the α configuration and is defined as

$$E_{z_k} = \frac{1}{2} \sum_{i=1}^{N} \sum_{j \neq i}^{N} \sum_{a}^{N_a} \sum_{b}^{N_b} H_k(z_i) U(r_{iajb}), \tag{25}$$

where $U(r_{iajb})$ is the sum of the 6-12 LJ and electrostatic energy contributions in the slab k, and $H_k(z_i)$ is a top-hat function with functional values of

$$H_k(z_i) = 1 \quad \text{for } z_k - \frac{\delta z}{2} < z_i < z_k + \frac{\delta z}{2},$$
$$H_k(z_i) = 0 \quad \text{otherwise}. \tag{26}$$

We adopt the definition of Ladd and Woodcock[42] and choose to assign in the slab centered on z_k two energy contributions: one contribution due to the energy between the molecules within the slab and a second contribution due to the energy of the molecules within the slab with those outside the slab. By using this definition, we respect the following condition:

$$\int_V dz_k U_{z_k} = E, \tag{27}$$

where E is the total configurational energy of the simulation box and V its volume. In Eqs. (23) and (24), the difficulty lies in the calculation of the local chemical potential (μ_{β,z_k}) at the β inverse temperature. To avoid additional simulations, we use a self-consistency approach consisting in calculating the chemical potential at the inverse temperature β. We apply an iterative process to resolve Eq. (28). Once the value of (μ_{β,z_k}) is obtained, we repeat a new iterative process for the calculation of the observable property as in Eq. (24). To summarize the different steps, the calculation of f_{l,z_k} [Eq. (23)] is first carried out, then we calculate $\langle \mu \rangle_{\beta,z_k}$ [Eq. (28)], and we finish with $\langle X \rangle_{\beta,z_k}$ using Eq. (24) as follows:

$$\langle \mu \rangle_{\beta,z_k} = \frac{\Sigma_i^R \Sigma_\alpha \mu_{i\alpha,z_k} (\Sigma_j^R N_j \exp(-((\beta_j - \beta) E_{i\alpha,z_k} - n_{i\alpha,z_k}(\beta_j \mu_{j,z_k} - \beta\langle\mu\rangle_{\beta,z_k}) - f_{j,z_k})))^{-1}}{\Sigma_i^R \Sigma_\alpha (\Sigma_j^R N_j \exp(-((\beta_j - \beta) E_{i\alpha,z_k} - n_{i\alpha,z_k}(\beta_j \mu_{j,z_k} - \beta\langle\mu\rangle_{\beta,z_k}) - f_{j,z_k})))^{-1}}, \tag{28}$$

where n_{α,z_k} is the number of molecules in the slab z_k for the α configuration. $E_{i\alpha,z_k}$ represents the total energy of the slab z_k calculated from the sum of the intrinsic contribution given by Eq. (25) and of the LRC part given by the following expression:

$$U_{\mathrm{LRC}}(z_k) = U_{\mathrm{LRC}}^{(1)}(z_k) + U_{\mathrm{LRC}}^{(2)}(z_k) = 2\pi\rho^2(z_k) V_s \int_{r_c}^{\infty} dr\, r^2 U_{\mathrm{LJ},m}(r) + \pi\rho(z_k) V_s \int_{r_c}^{\infty} dr \int_{-r}^{r} d\Delta\, z[\rho(z) - \rho(z_k)] r U_{\mathrm{LJ},m}(r). \tag{29}$$

B. Calculation of a local chemical potential

The calculation of the chemical potential μ allows us to check the local chemical equilibrium of a system where a nonuniformity of the density takes place along a specific direction. In the case of the constancy of the chemical potential throughout the z direction of the heterogeneity, we may use the decomposition of the system into open subsystems with constant local chemical potential.[3] Different techniques have been used for the calculation of the chemical potential. Among them, the original test particle insertion method of Widom[43] has been widely applied for the calculation of the chemical potential in homogeneous systems. This method consists in inserting a ghost particle randomly into a simulation box of N molecules and calculating the interaction energy of its ghost particle with the N molecules. As concerns the calculation of the chemical potential in heterogeneous systems, Widom[44] has changed the original version in such a way as to account for the dependence of μ on the local density ρ_{z_k}. However, in the case of systems involving both electrostatic interactions and high density, the test particle insertion can no longer be applied. One alternative consists in making the insertion easier by decomposing the move into two steps: the insertion of a LJ center and the calculation of the electrostatic contribution resulting from a perturbation process. This method gives accurate results for homogeneous systems, but the extension of this methodology for heterogeneous systems is time consuming due to the need for obtaining a profile of the chemical potential along the axis where a nonuniformity exists. Instead, we perform an insertion scheme with biased positions and orientations[45–47] for the calculation of the local chemical potential in a heterogeneous system. This method involves in a first step the selection of an appropriate location for the center of mass of the considered inserted molecule by n test insertions of a LJ particle, whose properties depend on the type of molecule to be inserted. In a second step, m orientations are tested in the selected location, with the full potential defined as the sum of the LJ and electrostatic energy contributions. Within this formalism, the chemical potential is then given by

$$\mu = -kT \ln \left\langle \frac{1}{\Lambda^3} \frac{V}{N+1} W_{\mathrm{LJ}} W_{\mathrm{or}} \exp(-(\beta \Delta U_{\mathrm{cor}} - \beta \Delta U_{\mathrm{LJ}})) \right\rangle_{NVT} \tag{30}$$

with

$$W_{\mathrm{LJ}} = \left(\frac{1}{k} \sum_{i=1}^{k} \exp(-(\beta \Delta U_{\mathrm{LJ},i})) \right), \qquad W_{\mathrm{or}} = \left(\frac{1}{m} \sum_{j=1}^{m} \exp(-(\beta \Delta U_{j})) \right), \tag{31}$$

where Λ is the de Broglie thermal wavelength. $\langle \cdots \rangle_{NVT}$ indicates the canonical ensemble average, V is the volume of the system, and N is the total number of particles. W_{LJ} and W_{or} are the Rosenbluth factors associated with the selection of the test location and of the various orientations, respectively. ΔU_{LJ} is the energy variation corresponding to the test insertion of the LJ particle in the selected location and ΔU_{cor} represents the variation of the LRCs corresponding to the insertion of the molecule. ΔU in Eq. (31) denotes the sum of the LJ and electrostatic energy contributions.

In the case of a nonuniformity of the density along the z direction, we extend the expressions of Eqs. (30) and (31) to the following expressions:

$$\mu(z_k) = -kT \ln \left\langle \frac{1}{\Lambda^3} \frac{V_{z_k}}{N_{z_k}+1} W_{\mathrm{LJ},z_k} W_{\mathrm{or},z_k} \exp(-(\beta \Delta U_{\mathrm{cor},z_k} - \beta \Delta U_{\mathrm{LJ},z_k})) \right\rangle_{\mu_{z_k} V_{z_k} T_{z_k}}, \tag{32}$$

$$W_{\mathrm{LJ},z_k} = \left(\frac{1}{k} \sum_{i=1}^{k} \exp(-(\beta \Delta U_{\mathrm{LJ},i,z_k})) \right), \qquad W_{\mathrm{or},z_k} = \left(\frac{1}{m} \sum_{j=1}^{m} \exp(-(\beta \Delta U_{j,z_k})) \right), \tag{33}$$

where $\langle \cdots \rangle_{\mu_{z_k} V_{z_k} \beta}$ indicates the average ensemble in the grand canonical ensemble. In Eqs. (32) and (33), the definition of the different properties are similar to that given in Eqs. (30) and (31) except for the fact that these properties are calculated within each slab located at z_k.

We make the assumption that the average of the ratio $\langle \rho(z_k) / W_{\mathrm{LJ},z_k} W_{\mathrm{or},z_k} \exp(-(\beta \Delta U_{\mathrm{cor},z_k} - \beta \Delta U_{\mathrm{LJ},z_k})) \rangle$ can be replaced by the ratio of the two averages $\langle \rho(z_k) \rangle / \langle W_{\mathrm{LJ},z_k} W_{\mathrm{or},z_k} \exp(-(\beta \Delta U_{\mathrm{cor},z_k} - \beta \Delta U_{\mathrm{LJ},z_k})) \rangle$. This approximation has been validated in a previous study,[3] where we checked that the difference between these averages is 10^{-5} unit. The resulting local chemical potential along the z direction can be calculated via the following expression:

$$\begin{aligned} \mu(z_k) &= kT \ln \langle \rho(z_k) \Lambda^3 \rangle_{\mu_{z_k} V_{z_k} T_{z_k}} \\ &\quad - kT \ln \langle W_{\mathrm{LJ},z_k} W_{\mathrm{or},z_k} \exp(-(\beta \Delta U_{\mathrm{cor},z_k} \\ &\quad - \beta \Delta U_{\mathrm{LJ},z_k})) \rangle_{\mu_{z_k} V_{z_k} T_{z_k}} \\ &= \mu_{\mathrm{id}}(z_k) + \mu_{\mathrm{ex}}(z_k), \end{aligned} \tag{34}$$

where $\mu_{\mathrm{id}}(z_k) + \mu_{\mathrm{ex}}(z_k)$ are the local ideal and excess contributions of the chemical potential. To take into account the LRC of the local chemical potential, we use the local expressions proposed by Guo and Lu,[35]

$$\begin{aligned} \mu_{\mathrm{LRC}}(z_k) &= 4\pi \rho(z_k) \int_{r_c}^{\infty} dr\, r^2 U_{\mathrm{LJ},m}(r) \\ &\quad + 2\pi \int_{r_c}^{\infty} dr \int_{-r}^{r} d\Delta z \sum_{i=-N_s/2}^{N_s/2} [\rho(z_{k-i}) \\ &\quad - \rho(z_{k-i+1})] r U_{\mathrm{LJ},m}(r). \end{aligned} \tag{35}$$

Finally, the total chemical potential is expressed as the sum of $\mu_{\mathrm{id}}(z_k)$, $\mu_{\mathrm{ex}}(z_k)$, and $\mu_{\mathrm{LRC}}(z_k)$.

TABLE I. CO_2 force field (Ref. 49) and description of the system.

	CO_2 potential parameters		
	σ (Å)	ϵ (K)	Charge (e)
C	2.757	28.129	+0.6512
O	3.033	80.507	−0.3256
C═O distance (Å)			1.149
O═C═O angle (deg)			180

MC parameters	
$L_x=L_y$ (Å)	25.4
L_z (Å)	150.8
$\mathbf{h}_x^{max}=\mathbf{h}_y^{max}$ ($Å^{-1}$)	9
$\mathbf{h}_z^{max}$ ($Å^{-1}$)	41

IV. RESULTS AND DISCUSSIONS

We apply the different techniques presented here for the calculation of the surface tension of the liquid-vapor interface of carbon dioxide. The simulation box is a rectangular parallelepipedic box of dimensions $L_xL_yL_z$ ($L_x=L_y$) with ($N=512$) CO_2 molecules. The details of the geometry of the system are given in Table I. The periodic boundary conditions are applied in the three directions. MC simulations are performed in the *NVT* ensemble. Each cycle consists of N randomly selected moves with fixed probabilities. Two types of MC moves are performed with probabilities of 0.5 each: the translation of the center of mass of a random molecule and the rotation of a randomly selected molecule around its center of mass.

The initial configuration has been built by placing N molecules on the nodes of a fcc lattice included in a cubic box with random orientations. MC simulations in the *NpT* ensemble have been performed first on this bulk monophasic fluid configuration. The dimension of the resulting box has been increased along the z axis by placing two empty cells on both sides of the bulk liquid box. A typical MC run consists of 200 000 cycles for equilibration and 200 000 cycles for the production phase.

The thermodynamic properties are calculated every ten cycles, leading to the storage of 20 000 configurations. The statistical errors for these properties are estimated using the jackknife method.[48] This method uses four superblocks which are formed by combining three blocks of 5000 configurations. As the geometry of the system shows a heterogeneity along the axis normal to the interface (z axis), we expect thus a dependence of the thermodynamic properties only in this direction. We have therefore calculated the local thermodynamic properties and their LRC as a function of z_k by splitting the cell into slabs of width δz.

The CO_2 molecule is described using the rigid version of the Harris–Yung potential[49] with three LJ centers and three electrostatic charges (see Table I). The carbon-oxygen bond lengths are fixed and equal to 1.149 Å and the carbon dioxide molecule has a fixed OCO angle of 180°. The intermolecular interactions are modeled using the 6–12 LJ potential. The unlike interatomic interactions are calculated using the Lorentz–Berthelot combining rules, i.e., a geometric combining rule for the energy and an arithmetic combining rule for the atomic size. We use a relatively small cutoff of 12 Å to make the two-phase simulations in line with those carried out in the Gibbs ensemble Monte Carlo (GEMC) method.[50–52] In this case, the use of the LRCs to be added to the interfacial properties is meaningful. We have also shown[4] that the value of the surface tension calculated from MC simulations becomes independent of the cutoff radius once the LRCs are included. For systems with electrostatic interactions calculated using the Ewald technique,[53,54] we take $\mathbf{h}_x^{max}=\mathbf{h}_y^{max}=9$ and $\mathbf{h}_z^{max}=41$ with respect to both the ratio of the box dimensions and the convergence of the reciprocal space contribution of the surface tension.

The calculation of the surface tension from the simulation of two-phase systems can be affected by the use of both periodic boundary conditions and small surface areas.[5,55] These recent works established an oscillatory function of the intrinsic part of the surface tension of LJ fluids for small surface areas and a constant value of the surface tension with larger surface areas. Beyond an interfacial area of $(7\times7\sigma^2)$, where σ is the diameter of the LJ particle, we observe that the maximum variation in the intrinsic part of the surface tension does not exceed 15% of the constant value of γ. The interfacial area used in this work approximately corresponds to the value of $(7\times7\sigma^2)$. Let us recall that we must maintain an objective of computational efficiency for the two-phase simulation with respect to the simulation carried out with the GEMC methods.[50] As a result, we aim to find a compromise between the system size and the CPU time. Then we evaluate the impact of the box dimensions on the calculation of the surface tension by keeping the surface area constant and changing the L_z dimension, and vice versa. Direct Monte Carlo simulations were then performed for $N=512$, 768, and 1024 system sizes for the liquid-vapor interface of CO_2 at $T=238$ K. The different contributions of the surface tensions are given in Table II for the KB, IK, TA, and KBZ approaches. We do not observe a trend of the surface tension over this range of system sizes. The results show that the total surface tension is a little dependent on the system size for the systems studied here due to the fact that the changes in the surface tension are within the fluctuations estimated using the variation in the block averages. Additionally, the variations in the surface tension are comparable to those induced by the calculation of γ using different definitions. The magnitude of the fluctuations of the surface tension can be attributed to the fact that we are simulating molecular systems interacting through dispersion-repulsion and electrostatic interactions in contrast to those obtained in the simulation of LJ fluids. These fluctuations are of the same order of magnitude as those induced by the dependence of the surface tension with the surface area beyond an area of $(7\times7\sigma^2)$. The fact that the surface tension remains unchanged within the statistical fluctuations when increasing the system size has already been observed for the calculation of the surface tension of water.[18] It was also established by Guo and Lu[35] that taking into account the LRC's contributions to the configurational energy in the Metropolis scheme allows us to obtain reliable surface tensions with a smaller total

TABLE II. Surface tension values (mN m^{-1}) of carbon dioxide at T=238 K calculated from MC simulations using different box dimensions and different numbers of molecules. The LRC contribution and the total surface tension are given for each method. The subscripts give the accuracy of the last decimal(s), i.e., 11.8_{10} means 11.8 ± 1.0. The experimental surface tensions (Ref. 57) ($\gamma_{expt.}$) are reported for comparison.

T (K)	γ_{KB}		γ_{IK}		γ_{TA}		γ_{KBZ}		
	γ_{LRC}	γ_{TOT}	γ_{LRC}	γ_{TOT}	γ_{LRC}	γ_{TOT}	γ_{LRC}	γ_{TOT}	$\gamma_{expt.}$
				N=512, L_x=L_y=25.4 Å, L_z=150.8 Å					
238	3.1_2	11.8_{10}	2.5_5	11.5_{10}	1.8_5	11.7_{10}	2.1_3	11.0_{10}	12.0
				N=768, L_x=L_y=32.4 Å, L_z=150.8 Å					
238	3.0_2	11.9_{10}	2.1_5	11.8_{10}	2.3_5	12.6_{10}	2.0_3	11.9_{10}	12.0
				N=1024, L_x=L_y=25.4 Å, L_z=200.8 Å					
238	3.5_2	12.1_{10}	2.2_5	11.5_{10}	2.1_5	11.8_{10}	1.9_3	11.9_{10}	12.0
				N=1024, L_x=L_y=32.4 Å, L_z=200.8 Å					
238	2.9_1	11.9_{10}	2.6_3	11.2_{10}	1.7_4	11.8_{10}	2.0_3	11.2_{10}	12.0

number of molecules. We have also underlined this point in the case of a previous work[4] dealing with the calculation of surface tensions of *n*-alkanes.

Before paying further attention to the MHR results, we have tested the single histogram reweighting formalism on the calculation of the surface tension of CO_2 at 248 K from the reference temperature of 238 K. From the surface tension calculated by MC simulation using the IK definition at 238 K (γ_{IK}=11.5 mN^{-1}), we find that the single histogram reweighting method gives γ_{IK}=12.5 mN^{-1} at 248 K. We observe that this methodology is not appropriate and leads to a value of surface tension that increases as the temperature increases. The surface tensions at 248 K resulting from MC simulation and from experimental measurements are equal to 10.8 and 9.7 mN^{-1}, respectively.

In the cases of the MHR and MHRS methods, we have tested two types of calculations: one involving three reference temperatures (238, 248, and 298 K) and a second using seven reference temperatures (238, 248, 258, 268, 278, 288, and 298 K). Figure 1 shows the calculated surface tensions using the MHR technique with three and seven reference temperatures. The experimental and calculated surface tensions at seven reference temperatures are reported in Table III and presented in Fig. 1 for comparison. We observe that the use of three reference temperatures does not lead to a good reproduction of the surface tensions in the range of temperatures studied. Calculating the surface tension with seven reference temperatures decreases the discrepancy but does not allow a good prediction of γ for temperatures lower than the lowest reference temperature, i.e., 238 K, because this zone is outside the temperature range covered by the reference temperatures. No extrapolation attempts have been performed in the high temperature region because calculations are restricted to temperatures below the critical temperature of CO_2, which is 304 K. Figure 1 shows the high sensitivity of the MHR technique to the convergence quality of the reference MC simulations. A slight overestimate or underestimate of a single point can strongly affect the global trend of the surface tension evolution with temperature. The challenge of this work is to combine a relatively small number of reference temperatures and a good prediction of the surface tensions. To do so, we apply our MHRS methodology, which consists in applying the MHR technique to local surface tensions. Such calculations are based on the calculation of the local chemical potential.

Figure 2(a) shows the profile of the total chemical potential calculated from the sum of the contributions given in Eqs. (34) and (35) at 248 K. As expected for a system at chemical equilibrium, we observe that the total chemical potential is constant throughout the z direction. We have already shown that the total chemical potential is independent of z_k in the case of a liquid-vapor interface of *n*-alkanes.[3] In

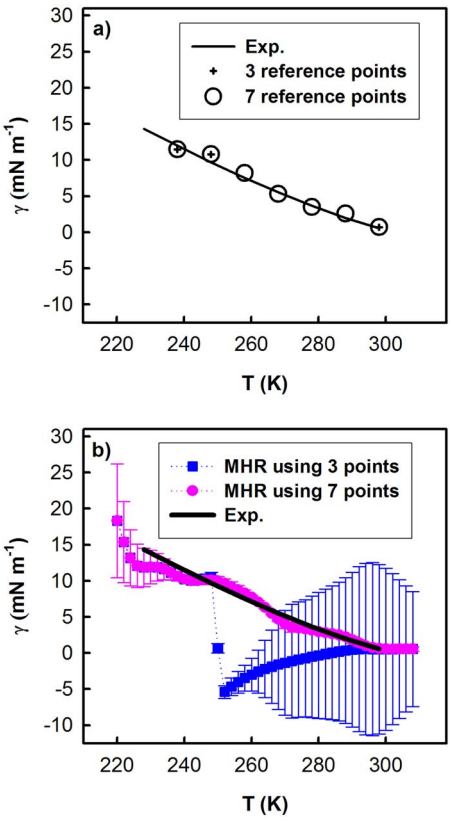

FIG. 1. (Color online) (a) Surface tension values of the liquid vapor of CO_2 calculated from MC simulations and experiments. The calculated points constitute the sets of three and seven reference temperatures. (b) Surface tensions of CO_2 calculated from the MHR technique with three and seven reference temperatures as indicated in the legend.

TABLE III. LRCs and intrinsic and total contributions of the surface tension (mN m^{-1}) calculated from MC simulations. Experimental values (Ref. 57) are given for comparison. The subscript indicates the accuracy of the last decimal(s). The number 11.5_{10} means 11.5 ± 1.0.

T (K)	$\gamma_{IK,LRC}$[a]	γ_{IK}[b]	γ_{Total}	$\gamma_{Expt.}$
238	2.5_5	9.0_{10}	11.5_{10}	12.0
248	2.2_5	8.6_{10}	10.8_{10}	9.7
258	1.9_5	6.3_{10}	8.2_{10}	7.6
268	1.5_5	3.8_{10}	5.3_{10}	5.5
278	1.1_5	2.4_5	3.5_5	3.6
288	0.8_5	1.8_6	2.6_6	2.0
298	0.4_5	0.3_1	0.7_5	0.6

[a]Equation (1).
[b]Equation (3).

the case of a carbon dioxide liquid-vapor interface, let us recall that the calculation requires more sophisticated algorithms due to the insertion of a molecule requiring the calculation of electrostatic energy contributions. We also checked that the total chemical potential recalculated from Eq. (28) by using the MHRS methodology respects the chemical equilibrium in the two-phase system. In the calculation of $\langle \mu \rangle_{\beta,z_k}$ from Eq. (28), we need to save μ_{j,z_k}, which represents the chemical potential of a configuration j at a slab k. The calculation of μ in Eq. (34) exhibits the presence of a logarithm of the average of an exponential term. It means that the operational expression of μ of Eq. (34) cannot be decomposed into instantaneous values. We decided to apply the MHRS methodology on the term $W_{\mathrm{LJ},z_k} W_{\mathrm{or},z_k} \exp(-(\beta \Delta U_{\mathrm{cor},z_k} - \beta \Delta U_{\mathrm{LJ},z_k}))$ and to use this term instead of μ in Eq. (28). Figure 2(b) displays the profile of the excess part of the chemical potential at 248 K. From this curve, it is then possible to extract the excess chemical potential of the vapor and liquid phases by fitting the profile with a hyperbolic tangent function defined as

$$\mu_{\mathrm{ex}}(z_k) = \frac{1}{2}(\mu_{\mathrm{ex}}^l + \mu_{\mathrm{ex}}^v) - \frac{1}{2}(\mu_{\mathrm{ex}}^l - \mu_{\mathrm{ex}}^v)\tanh\left(\frac{z - z_o}{d}\right), \quad (36)$$

where μ_{ex}^l and μ_{ex}^v are the excess chemical potentials of the liquid and vapor phases, z_o is the position of the Gibbs dividing surface, and d is an approximate measure of the thickness of the interface. We presented in Fig. 2(c) the $\Delta\mu_{\mathrm{ex}} = \mu_{\mathrm{ex}}^l - \mu_{\mathrm{ex}}^v$ contribution calculated from Eq. (36). We compared the resulting values to the expression derived by Ben-Naim *et al.*[56] $[\Delta\mu_{\mathrm{ex}} = -k_B T \ln(\rho^l/\rho^v)]$, where ρ^l and ρ^v are the experimental coexisting densities of the liquid and vapor phases, respectively. We observed that the calculated $\Delta\mu_{\mathrm{ex}}$ term matches quite well with the experimental value, indicating the correctness of the extension of the bias insertion scheme to a slab version in a two-phase system. Additionally, we presented on the right axis of Fig. 2(c) the total chemical potential calculated from both the GEMC simulations of homogeneous liquid and vapor phases using Eq. (30) and the direct MC simulations of the corresponding two-phase system using Eq.(34). We checked that the calculated chemical potential are similar within the error bars. We also checked that the calculation of the local chemical potential using the

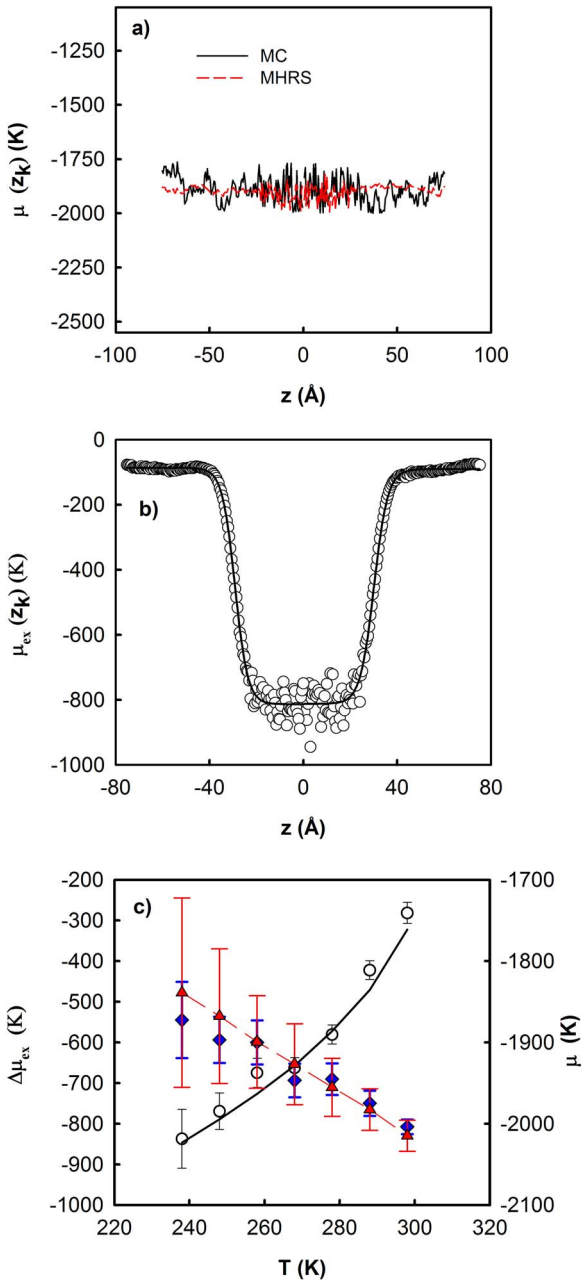

FIG. 2. (Color online) (a) Total chemical potential profiles of the CO_2 liquid-vapor interface at 248 K calculated from the sum of the contributions of Eqs. (34) and (35) and from the MHRS procedure with Eq. (28). (b) Excess chemical potential profiles with parts calculated from the Rosenbluth scheme [Eq. (32)] and from the fit using Eq. (36). (c) Total chemical potential values (right axis) calculated from GEMC simulations using Eq. (30) (▲) and from the two-phase simulation using Eqs. (34) and (35) (◆). The difference of excess chemical potential values (left axis) calculated using Eq. (36) (○) and using $\Delta\mu_{ex} = -k_B T \ln(\rho^l/\rho^v)$ (solid line), where ρ^l and ρ^v are the experimental coexisting densities (Ref. 57) of the liquid and vapor phases, respectively.

configurational-bias scheme leads to the constancy of the chemical potential at each z_k and provides values in agreement with the corresponding values[57] derived from experimental densities. We now focus on the prediction of the surface tension using the MHRS technique.

Figure 3 shows the surface tension values calculated using the methodology developed in this paper using either three or seven reference temperatures. Interestingly, we ob-

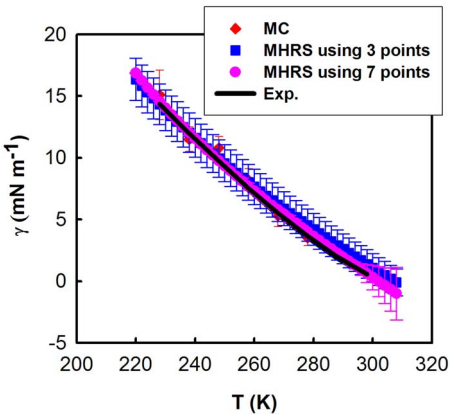

FIG. 3. (Color online) Surface tension values of the liquid vapor of CO_2 calculated with the MHRS methodology using different procedures as indicated in the legend.

serve that the MHRS methodology gives surface tensions in line with the experimental values even in the case of three reference temperatures. We conclude that the adopted methodology (MHRS), which consists in calculating local surface tensions from local configurational energy and local chemical potential, is efficient even in the case of using a relatively small number of reference temperatures. It was a prerequisite to make the MHRS methodology an efficient and powerful technique for the surface tension calculation. When the number of reference points is fixed to 7, we observed that the MHRS significantly improves the calculated values, leading to surface tensions in excellent agreement with the experimental ones.[57]

V. CONCLUSIONS

We have extended the standard MHR method to a new version that allows us to calculate local surface tensions from local configurational energies and local chemical potentials. The different steps essential to the use of the MHRS method have been discussed and the operational expressions of the local chemical potential, of the local configurational energies, and of their LRCs have been presented. The results of this new technique, called MHRS in this paper, are very promising. The calculated surface tensions of the liquid-vapor interface of carbon dioxide are found to be in excellent agreement with the experimental ones even in the case of a small number of reference temperatures. We have also checked the chemical equilibrium of the system by presenting the profile of the total chemical potential calculated from the configurational-bias scheme.

The MHRS methodology can be applied to different approaches for the calculation of the surface tension. However, these approaches must allow a local definition of the surface tension as, for example, the TA (Ref. 3) and the KBZ (Ref. 28) methods.

ACKNOWLEDGMENTS

One of the authors (A.G.) is grateful to Carlos Draghi Nieto and Javier Pérez-Pellitero for stimulating discussions.

APPENDIX A: RELATIONSHIP BETWEEN $\Xi_{\mu,V,\beta}$ AND $\Pi_z \Xi(\mu_{z_k}, V_{zk}, \beta)$

The local partition function in the grand canonical ensemble can be expressed as

$$\Xi(\mu_{z_k}, V_{zk}, T_{z_k}) = \sum_N \exp(\beta\mu N_{z_k}) Q(N_{z_k}, V_{zk}, T_{z_k}) = \sum_N \sum_l \exp(\beta\mu_{z_k} N_{z_k}) \exp(-\beta U_l^{N_{z_k}}). \tag{A1}$$

The product for z_k is equal to

$$\prod_{z_k} \Xi(\mu_{z_k}, V_{z_k}, T_{z_k}) = \prod_{z_k} \sum_{N_{z_k}} \exp(\beta\mu_{z_k} N_{z_k}) Q(N_{z_k}, V_{z_k}, T_{z_k}) \tag{A2a}$$

$$= \left[\sum_{N_{z_1}} \exp(\beta\mu_{z_1} N_{z_1}) Q(N_{z_1}, V_{z_1}, T_{z_1}) \right] \times \left[\sum_{N_{z_2}} \exp(\beta\mu_{z_2} N_{z_2}) Q(N_{z_2}, V_{z_2}, T_{z_2}) \right] \tag{A2b}$$

$$= [\exp(\beta\mu_{z_1} N_{z_1}^1) Q(N_{z_1}, V_{z_1}, T_{z_1}) + \exp(\beta\mu_{z_1} N_{z_1}^2) Q(N_{z_1}, V_{z_1}, T_{z_1})] \times [\exp(\beta\mu_{z_2} N_{z_2}^1) Q(N_{z_2}, V_{z_2}, T_{z_2}) + \exp(\beta\mu_{z_2} N_{z_2}^2) Q(N_{z_2}, V_{z_2}, T_{z_2})] \times \cdots. \tag{A2c}$$

In this expression, the superscripts 1 and 2 indicate the various sampled states, whereas the subscripts denote the number of the slab. When we consider the terms satisfying the constraints relative to the total energy and to the total number of molecules ($N = \Sigma_{i=1}^{N_s} N_{z_i}$ and $\int_V dz_k U_{z_k} = U$) and the fact that the local chemical potential and the local temperature are constant at each z_k and equal to μ and T, respectively, we obtain

$$\prod_{z_k} \Xi(\mu_{z_k}, V_{zk}, T_{z_k}) = \sum_N \left[\exp(\beta\mu N) \prod_{z_k} Q(N_{z_k}, V_{zk}, T_{z_k}) \right]. \tag{A3}$$

By following the same reasoning and using the same constraints, we can write $\Pi_{z_k} Q(N_{z_k}, V_k, T_{z_k}) \simeq Q(N, V, T)$. This allows us to write the following expressions:

$$\prod_{z_k} \Xi(\mu_{z_k}, V_{zk}, T_{z_k}) \simeq \sum_N [\exp(\beta\mu N) Q(N, V, T)], \tag{A4}$$

$$\prod_{z_k} \Xi(\mu_{z_k}, V_{zk}, T_{z_k}) \simeq \Xi(\mu, V, T). \tag{A5}$$

Equation (A5) allows us to assume the existence of a local partition function. The relationship between $\gamma_{\mu,V,T}$ and $\gamma_{N,V,T}$ is established in Appendix B.

APPENDIX B: TRANSFORMATION OF $\gamma_{\mu,V,T}$ TO $\gamma_{N,V,T}$

The demonstration of the relationship between $\Xi(\mu,V,T)$, $N_{\mathrm{ref}}Q(\mu,V,T)$, and $Q(N_{\mathrm{ref}},V,T)$ has been carried out by Gloor *et al.*[27] Here N_{ref} is the number of particles in the case of a restricted grand canonical partition function $\Xi(\mu,V,T)(N_{\mathrm{ref}})$ for systems containing just N_{ref} particles. The partition function in canonical ensemble for N_{ref} is equal to

$$Q(N_{\mathrm{ref}},V,T)=\Xi(\mu,V,T)(N_{\mathrm{ref}})\exp(-(\beta\mu N_{\mathrm{ref}})) \tag{B1a}$$

$$=\Xi(\mu,V,T)\exp(-(\beta\mu N_{\mathrm{ref}}))P(N_{\mathrm{ref}}), \tag{B1b}$$

where $\Xi(\mu,V,T)$ is the grand canonical partition function and $P(N_{\mathrm{ref}})$ is the probability density of finding exactly N_{ref} in any element of configurational space $d_{\mathbf{r}^{N_{\mathrm{ref}}}}$. By using this definition, we can express the product of the local partition functions of Eq. (A5) as

$$\prod_{z_k}\Xi(\mu,V_{zk},T)\simeq\Xi(\mu,V,T)\simeq\frac{\Xi(\mu,V,T)(N_{\mathrm{ref}})}{P(N_{\mathrm{ref}})}\simeq\frac{Q(N_{\mathrm{ref}},V,T)\exp((\beta\mu N_{\mathrm{ref}}))}{P(N_{\mathrm{ref}})}. \tag{B2}$$

We now consider the calculation of the macroscopic surface tension as a perturbation of the free energy with respect to the surface. $\gamma=(\partial F/\partial A)_{\mu VT}$. If we use a finite difference to calculate γ, the free energy can be expressed by a partition function according to a statistical mechanics definition,

$$\sum_{z_k}\gamma_{\mu_{z_k},V_{zk},T}=-\frac{kT}{2\Delta A}\ln\frac{\Pi_{z_k}\Xi(\mu,V_{z_k},T,A)}{\Pi_{z_k}\Xi(\mu,V_{z_k},T,A+\Delta A)}=-\frac{kT}{2\Delta A}\ln\prod_{z_k}\frac{\Xi(\mu,V_{z_k},T,A)}{\Xi(\mu,V_{z_k},T,A+\Delta A)} \tag{B3a}$$

$$\simeq-\frac{kT}{2\Delta A}\ln\left[\frac{\dfrac{Q(N_{\mathrm{ref}},V,T,A)\exp((\beta\mu N_{\mathrm{ref}}))}{P(N_{\mathrm{ref},A})}}{\dfrac{Q(N_{\mathrm{ref}},V,T,A+\Delta A)\exp((\beta\mu N_{\mathrm{ref}}))}{P(N_{\mathrm{ref},A+\Delta A})}}\right]. \tag{B3b}$$

The transformation for the change in the surface area conserves the volume of each slab. We suppose that the chemical equilibrium is maintained between the reference and the perturbed states and that the probabilities of finding the system in the configuration spaces $d_{\mathbf{r}^{N_{\mathrm{ref}}}}$ and $d_{\mathbf{r}'^{N_{\mathrm{ref}}}}$ are very close, where the $\mathbf{r}'^{N_{\mathrm{ref}}}$ represent the configurational space of the perturbed system,

$$\sum_{z_k}\gamma_{\mu z_k,V_{z_k},T}\simeq\gamma_{\mu,V,T}\simeq-\frac{kT}{2\Delta A}\ln\left[\frac{Q(N_{\mathrm{ref}},V,T,A)}{Q(N_{\mathrm{ref}},V,T,A+\Delta A)}\right]$$

$$\simeq\gamma_{N_{\mathrm{ref}},V,T}. \tag{B4}$$

[1] A. Trokhymchuk and J. Alejandre, J. Chem. Phys. **111**, 8510 (1999).
[2] F. Goujon, P. Malfreyt, J. M. Simon, A. Boutin, B. Rousseau, and A. H. Fuchs, J. Chem. Phys. **121**, 12559 (2004).
[3] C. Ibergay, A. Ghoufi, F. Goujon, P. Ungerer, A. Boutin, B. Rousseau, and P. Malfreyt, Phys. Rev. E **75**, 051602 (2007).
[4] F. Goujon, P. Malfreyt, A. Boutin, and A. H. Fuchs, J. Chem. Phys. **116**, 8106 (2002).
[5] P. Orea, J. Lopez-Lemus, and J. Alejandre, J. Chem. Phys. **123**, 114702 (2005).
[6] J. R. Errington, Phys. Rev. E **67**, 012102 (2003).
[7] J. R. Errington, J. Chem. Phys. **118**, 9915 (2003).
[8] K. Binder, Phys. Rev. A **25**, 1699 (1982).
[9] J. J. Potoff and A. Z. Panagiotopoulos, J. Chem. Phys. **112**, 6411 (2000).
[10] J. K. Singh, D. A. Kofke, and J. R. Errington, J. Chem. Phys. **119**, 3405 (2003).
[11] J. K. Singh and J. R. Errington, J. Phys. Chem. B **110**, 1369 (2006).
[12] E. M. Grzelak and J. R. Errington, J. Chem. Phys. **128**, 014710 (2008).
[13] A. M. Ferrenberg and R. H. Swendsen, Phys. Rev. Lett. **61**, 2635 (1988).
[14] A. M. Ferrenberg and R. H. Swendsen, Phys. Rev. Lett. **63**, 1195 (1989).
[15] V. K. Shen, R. D. Mountain, and J. R. Errington, J. Phys. Chem. B **111**, 6198 (2007).
[16] V. K. Shen and J. R. Errington, J. Phys. Chem. B **124**, 024721 (2006).
[17] M. P. Moody and P. Attard, J. Phys. Chem. B **120**, 1892 (2004).
[18] J. Alejandre, D. J. Tildesley, and G. A. Chapela, J. Chem. Phys. **102**, 4574 (1995).
[19] J. G. Kirkwood and F. P. Buff, J. Chem. Phys. **17**, 338 (1949).
[20] F. B. Buff, Z. Elektrochem. **56**, 311 (1952).
[21] A. G. McLellan, Proc. R. Soc. London, Ser. A **213**, 274 (1952).
[22] A. G. McLellan, Proc. R. Soc. London, Ser. A **217**, 92 (1953).
[23] J. S. Rowlinson and B. Widom, *Molecular Theory of Capillarity* (Clarendon, Oxford, 1982).
[24] J. H. Irving and J. G. Kirkwood, J. Chem. Phys. **18**, 817 (1950).
[25] J. P. R. B. Walton, D. J. Tildesley, and J. S. Rowlinson, Mol. Phys. **48**, 1357 (1983).
[26] J. P. R. B. Walton, D. J. Tildesley, and J. S. Rowlinson, Mol. Phys. **58**, 1013 (1986).
[27] G. J. Gloor, G. J. Jackson, F. J. Blas, and E. Miguel, J. Chem. Phys. **123**, 134703 (2005).
[28] A. Ghoufi, F. Goujon, V. Lachet, and P. Malfreyt, Phys. Rev. E **77**, 031601 (2008).
[29] F. P. Buff, A. Lowet, and F. H. Stillinger, Phys. Rev. Lett. **15**, 621 (1965).
[30] A. Milchev and K. Binder, J. Chem. Phys. **124**, 024721 (2006).
[31] A. E. Ismail, G. S. Grest, and M. J. Stevens, J. Chem. Phys. **125**, 014702 (2006).
[32] E. Salomons and M. Mareschal, J. Phys.: Condens. Matter **3**, 3645 (1991).
[33] E. M. Blokhuis, D. Bedeaux, C. D. Holcomb, and J. A. Zollweg, Mol. Phys. **85**, 665 (1995).
[34] M. Mecke and J. Winkelmann, J. Chem. Phys. **107**, 9264 (1997).
[35] M. Guo and B. C. Y. Lu, J. Chem. Phys. **106**, 3688 (1997).
[36] M. Mecke, J. Winkelmann, and J. Fischer, J. Chem. Phys. **110**, 1188 (1999).
[37] J. Janecek, J. Phys. Chem. B **110**, 6264 (2006).
[38] Z. W. Salsburg, J. D. Jacobson, W. Fickett, and W. W. Wood, J. Chem. Phys. **30**, 65 (1959).

[39] J. Pérez-Pellitero, P. Ungerer, G. Orkoulas, and A. D. Mackie, J. Chem. Phys. **125**, 054515 (2006).
[40] J. Pérez-Pellitero, P. Ungerer, and A. D. Mackie, J. Phys. Chem. B **111**, 4460 (2007).
[41] W. Shi and K. Johnson, Fluid Phase Equilib. **187–188**, 171 (2001).
[42] A. J. C. Ladd and L. V. Woodcock, Mol. Phys. **2**, 611 (1978).
[43] B. Widom, J. Chem. Phys. **39**, 2808 (1963).
[44] B. Widom, J. Chem. Phys. **19**, 563 (1978).
[45] D. Frenkel and B. Smit, Mol. Mater. **75**, 983 (1992).
[46] G. Moogi, D. Frenkel, and B. Smit, J. Phys.: Condens. Matter **4**, L255 (1992).
[47] E. Bourasseau, P. Ungerer, and A. Boutin, J. Phys. Chem. B **106**, 5483 (2002).
[48] B. Efron, *The Jackknife, the Bootstrap, and Other Resampling Plans* (SIAM, Philadelphia, 1982).
[49] J. G. Harris and K. H. Yung, J. Phys. Chem. **99**, 12021 (1995).
[50] A. Z. Panagiotopoulos, Mol. Phys. **67**, 813 (1987).
[51] A. Z. Panagiotopoulos, N. Quirke, M. Stapleton, and D. J. Tildesley, Mol. Phys. **63**, 527 (1988).
[52] A. Z. Panagiotopoulos, Mol. Simul. **9**, 1 (1992).
[53] M. P. Allen and D. J. Tildesley, *Computer Simulation of Liquids* (Clarendon, Oxford, 1989).
[54] E. R. Smith, Proc. R. Soc. London, Ser. A **375**, 475 (1981).
[55] J. R. Errington and D. A. Kofke, J. Chem. Phys. **127**, 174709 (2007).
[56] A. Ben-Naim and Y. Marcus, J. Chem. Phys. **81**, 2016 (1984).
[57] Data taken from the saturation properties of carbon dioxide at http://webbook.nist.gov.